J Nanopart Res (2013) 15:1969
DOI 10.1007/s11051-013-1969-7

RESEARCH PAPER

Structural and magnetic properties of Er-doped $BiFeO_3$ nanoparticles

Jianguo Zhao · Shijiang Liu · Weiying Zhang · Zhaojun Liu · Zhongli Liu

Received: 28 January 2013 / Accepted: 22 August 2013 / Published online: 3 September 2013

Abstract In this work, $Bi_{1-x}Er_xFeO_3$ ($x = 0.05$–0.25) nanoparticles were prepared by sol–gel method. X-ray diffraction and Raman analysis show that the structure of Er-doped $BiFeO_3$ changes from rhombohedral lattice to orthorhombic one by increasing x. The remnant magnetization of the $Bi_{1-x}Er_xFeO_3$ is significantly higher than those in $BiFeO_3$ doped with non-magnetically rare-earth and it increases with increasing Er concentration. The enhanced magnetization was attributed to the suppression of the cycloidal spin structure by Er^{3+} substitution and the ferromagnetic interaction between Fe^{3+} and Er^{3+} ions. The variation of the magnetization with temperature is also discussed.

Keywords Er-doped $BiFeO_3$ · Nanoparticles · Raman · Magnetic properties

Introduction

Multiferroic materials, especially those exhibiting ferroelectricity and ferromagnetism simultaneously, have been widely studied in recent years, due to their potential applications in data storage, spin valves, sensors, spintronics, microelectronic devices, etc. (Scott 2007; Allibe et al. 2012; Giang et al. 2012; Bhushan et al. 2012; Ramesh and Spaldin 2007). The interaction between the electric and magnetic subsystems can manifest itself as the giant magnetoelectric (ME) effect and the effect of mutual influence of the polarization and magnetization (Hur et al. 2009). Among all known multiferroics materials, $BiFeO_3$ is the most promising for room temperature ME applications, as it possesses high ferroelectric Curie temperature ($T_C \sim 1103$ K) and high G-type antiferromagnetic Neel temperature ($T_N \sim 643$ K) (Wang et al. 2003; Seshadri and Hill 2001). Superimposed on this antiferromagnetic ordering there is a cycloidal modulation with a wavelength of 62 nm. Consequently, its remnant magnetization and potential ME effect both vanish macroscopically, leading to a weak quadratic ME behavior rather than a strong linear ME behavior (Lebeugle et al. 2008).

Although $BiFeO_3$ has been extensively studied in recent years, some difficulties have limited its development. One of them is how to derive ferromagnetism in the canted G-type antiferromagnetic order with the space-modulated spin structure (Yuan et al. 2006). Recently, doping $BiFeO_3$ with a foreign atom at either A or B site of the $BiFeO_3$ lattice has been shown to play an important role in improving its ferromagnetism. For example, substituting Bi^{3+} with rare-earth elements, such as Gd^{3+}, Sm^{3+}, Dy^{3+}, etc., resulted in remarkable

J. Zhao · S. Liu · W. Zhang · Z. Liu · Z. Liu
School of Physics and Electronic Information, Luoyang Normal College, Luoyang 471022, Henan, People's Republic of China

J. Zhao (✉) · S. Liu · W. Zhang · Z. Liu · Z. Liu
Luoyang Key Laboratory of Laser Spectroscopy Technology, Henan, Luoyang 471022, Henan, People's Republic of China
e-mail: lynczjg@gmail.com

improvement of the ferroelectricity and ferromagnetism of $BiFeO_3$, which could possibly lead to enhanced ME effect (Guo et al. 2010; Khomchenko et al. 2010; Prashanthi et al. 2010). Minor attention has been paid to Er-doped $BiFeO_3$. Unlike other rare-earth cations, Er^{3+} ion is magnetically active and its coupling with Fe^{3+} ion can lead to the giant impact on the magnetization of $BiFeO_3$ even in the slight doping concentration.

Various wet chemical routes have been used to prepare $BiFeO_3$ nanostructures, such as hydrothermal synthesis, mechanochemical synthesis, sol–gel method, solid state reaction method, and others (Tan et al. 2012; Szafraniak et al. 2007; Wu et al. 2010; Xie et al. 2008). It is thought that the sol–gel method will be the very effective and controllable chemical route for future nanomaterial preparation. It has many advantages such as low cost, easy operation for doping, cleanliness, flexibility.

As there are few works devoted to the study of ferromagnetic properties of Er-substituted $BiFeO_3$, in this paper we prepared Er-doped $BiFeO_3$ nanoparticles by the sol–gel method. The crystal structures, morphologies, and magnetic properties were investigated in detail.

Experiments

Materials

All chemicals reagents were of analytical grade and used without further purification. $Fe(NO_3)_3{\cdot}9H_2O$ (99.999 %), $Er(NO_3)_3{\cdot}9H_2O$(99.999 %), and $Bi(NO_3)_3{\cdot}5H_2O$ (99.999 %) were purchased from J&K. 2-Methoxyethanol (≥99.0 %), acetic acid (99.5 %), and citric acid (99.5 %) were purchased from Tianjin chemical reagent 3 factory, China.

Sample preparation

$Bi_{1-x}Er_xFeO_3$ ($x = 0.05$, 0.1, 0.15, 0.2, and 0.25) nanoparticles were prepared by sol–gel method. For example, the $Bi_{0.95}Er_{0.05}FeO_3$ nanoparticles were prepared. First $Bi(NO_3)_3{\cdot}5H_2O$ (1 g) and $Er(NO_3)_3{\cdot}9H_2O$ (0.4807 g) were mixed in acetic acid (20 mL) under constant magnetic stirring for 2 h. Then $Fe(NO_3)_3{\cdot}9H_2O$ (0.8378 g), 2-methoxyethanol (20 mL), and citric acid (0.5 g) were added to the solution. After continuous stirring for 2 h, the solution was aged for 1 day, dried at 80 °C for 48 h, and grinded into powders. At last, the powders were sintered for 2 h in air at 800 °C. A series of samples of Er-doped $BiFeO_3$ nanoparticles ($Bi_{1-x}Er_xFeO_3$) with $x = 0.10$, 0.15, 0.20, and 0.25 were prepared by adopting the same procedure as mentioned above.

Characterization

The crystalline phases of the samples were determined by X-ray diffraction (XRD, Bruker D8 ADVANCE) with Cu K_α radiation ($\lambda = 1.54$ Å) and Raman scattering spectra (JY-HR800) using an Ar^+ laser (514.5 nm) as the excitation line. The microstructural properties of the samples were investigated by transmission electron microscopy (TEM) and high-resolution transmission electron microscopy (HRTEM, FEI Tecnai F30). Variable-temperature magnetization measurements under a magnetic field of 1,000 Oe and under both zero-field-cooled (ZFC) and field-cooled (FC) conditions were carried out using a Quantum Design SQUID MPMS XL-7 from 300 K down to 5 K. The dc hysteresis loops were collected using the same SQUID in magnetic field from 50,000 to −50,000 Oe at 5 and 300 K, respectively.

Results and discussion

The XRD patterns of all the samples in Fig. 1 reveal that all the peaks correspond to the reflections from (012), (104), (110), (006), (202), (024), (1116), (122), (018), and (214)/(300) planes of rhombohedral $BiFeO_3$, which are consistent with the standard reported values (JCPDS File No. 86-1518). XRD peak intensity ratios observed in above XRD patterns suggest polycrystalline behavior with good crystallinity. The average crystallite size of 10 % Er-doped $BiFeO_3$ sample estimated from XRD pattern by means of the Scherrer equation is 100 nm. With increasing Er concentration, two features should be noted in Fig. 1. (1) The intensity of some $Bi_{1-x}Er_xFeO_3$ diffraction peaks, that is, (006) and (018), become weak and tend to disappear. Although minor $Bi_{25}FeO_{40}$ could be detected, $Bi_{25}FeO_{40}$ is not ferromagnetic in nature at room temperature and thus so contributes little to the ferromagnetic properties observed in the Er-doped $BiFeO_3$ samples. (2) The peak splitting behavior in the samples decreases gradually. From the magnified

XRD patterns in the vicinity of 2θ around 32° (inset Fig. 1), we find that the separated (104) and (110) diffraction peaks tend to merge into a single broad peak with the Er concentration increasing and the peaks have a tendency to shift toward higher 2θ value. This result indicates that the rhombohedral structure is distorted by Er substitution, suggesting a structural phase transition at $x = 0.2$, which has also been observed in other rare-earth doped $BiFeO_3$ ceramics (Liu et al. 2010). The phase transition from rhombohedral to orthorhombic symmetry is attributed to the structural distortion resulting from the incorporation of Er ions into the lattice of $BiFeO_3$, because the ionic radius of Er is smaller than that of Bi.

The structural phase change in $Bi_{1-x}Er_xFeO_3$ was also investigated by the Raman measurements. Figure 2 shows the measured Raman scattering spectra of $Bi_{1-x}Er_xFeO_3$ ($x = 0.05$, 0.10, 0.15, 0.20, 0.25) nanoparticles sintered at 800 °C for 2 h in air. These mode frequencies were assigned according to the irreducible representation: $\Gamma = 4A_1 + 9E$, which is used to describe the Raman active modes of rhombohedral $R3c$ $BiFeO_3$ single crystal (Yuan et al. 2007). For $BiFeO_3$ nanoparticles with rhombohedral $R3c$ symmetry, there are 11 normal modes, including A_1—1, A_1—2, and A_1—3 modes with strong scattering intensities at 140, 172, and 220 cm^{-1}, respectively. The subsequent six peaks at 278, 339, 370, 474, 530, and 610 cm^{-1} can be assigned as E—2, E—3, E—4, E—5, E—6, and E—7 modes, respectively. The peak at 425 cm^{-1} that can be assigned as A_1—4 mode is too weak to be detected in our $Bi_{0.95}Er_{0.05}FeO_3$ sample and peak at 113 cm^{-1} that can be assigned as E—1 mode is overlapped with 140 cm^{-1} mode. However, with the increasing of Er doping concentration to 0.10, E—1, A_1—1, A_1—2, and A_1—3 modes governed by Bi–O covalent bonds are red shift indicating that the Er ions are entering into the Bi-sites of $BiFeO_3$. When the Er concentration is increasing to 0.15, the E—1, A_1—1, A_1—2 and A_1—3 modes are nearly disappearing, indicating that the phase transition occurs at this concentration. Moreover, a new peak at 310 cm^{-1} is observed, which may result from $ErFeO_3$ phase in the compounds. Such peaks have also been reported to exist in $RFeO_3$ (R = Gd, Dy, Nd, and Ho) (Gupta et al. 2002; Singh et al. 2008; Wu et al. 2009).

The crystalline structure of the 10 % Er-doped $BiFeO_3$ nanoparticles without stored in air is further examined by transmission electron microscopy and high-resolution transmission electron microscopy, as shown in Fig. 3. The average crystalline size is larger than the crystalline size obtained by the Scherrer equation from XRD patterns of 10 % Er-doped $BiFeO_3$. Such phenomenon has also been observed in other reported works and can be ascribed to the agglomeration of the particles (Selbach et al. 2007). We therefore conclude that the crystallite size found by the Scherrer equation is a reasonable estimate for the particle size. The rhombohedral perovskite structure of the 10 % Er-doped $BiFeO_3$ nanoparticles is

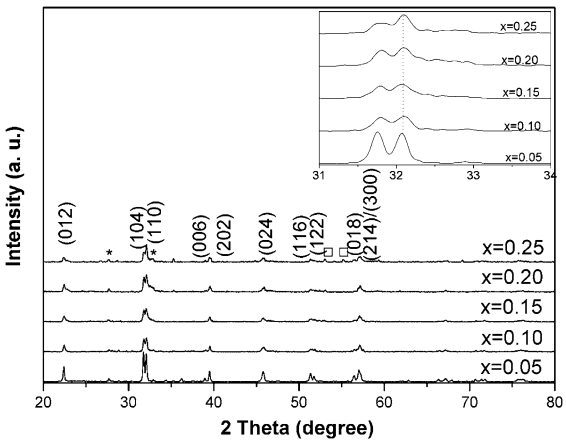

Fig. 1 XRD patterns of $Bi_{1-x}Er_xFeO_3$ ($x = 0.05$, 0.10, 0.15, 0.20, 0.25) nanoparticles sintered at 800 °C for 2 h. *Asterisks* $Bi_{25}FeO_{40}$ and *open square* $ErFeO_3$. *Inset* the magnified XRD patterns in the vicinity of 2θ around 32°

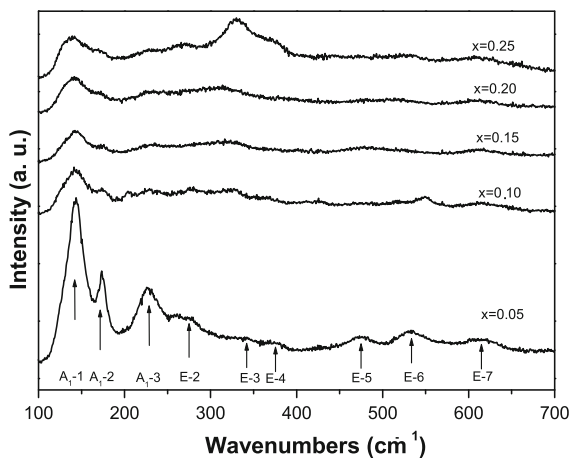

Fig. 2 Raman spectra of $Bi_{1-x}Er_xFeO_3$ ($x = 0.05$, 0.10, 0.15, 0.20, 0.25) nanoparticles sintered at 800 °C for 2 h and the active modes (*arrows*)

confirmed by HRTEM (Fig. 3b), where the lattice space is measured to be 0.278 nm along the (110) plane and 0.396 nm along the (012) plane, consistent with those reported for $BiFeO_3$ nanoparticles (Du et al. 2012; Park et al. 2007).

The room temperature magnetization (M–H) loops of all samples measured with the maximum magnetic field of 50 kOe are shown in Fig. 4a. In contrast to pure $BiFeO_3$ nanoparticles, which exhibit a linear magnetic field dependence on the magnetization, the Er-doped samples exhibit a hysteresis M–H behavior as expected. It can be seen that remnant magnetization (M_r) increases with the increase of Er content. This suggests that Er doping enhances the magnetic properties of $BiFeO_3$ nanoparticles.

The magnetization hysteresis (M–H) loops of $Bi_{1-x}Er_xFeO_3$ samples at 5 K are shown in Fig. 4b. The M_r values of samples are increasing with the increasing of x ($0.05 \leq x \leq 0.20$) and the M_r values of $Bi_{1-x}Er_xFeO_3$ with $x \leq 0.15$ are significantly less than that of $Bi_{0.8}Er_{0.2}FeO_3$. For the Er-doped $BiFeO_3$ samples, when $x \leq 0.15$, the Er substitution can only suppress but cannot destruct the spin cycloid, leading to small and limited increase of M_r value. These results are in accordance with other reports (Zhang et al. 2010; Li et al. 2013). However, when $x \geq 0.20$, the Er substitution results in structural phase transition wherein the spin cycloid might be destructed and homogeneous spin structure formed, so that the latent magnetization locked within the cycloid might be released and significant increased M_r value is observed. When the Er concentration is $x = 0.25$, the M_r value is decreasing. This could be because of the fact that with increase in Er concentration, formation of $ErFeO_3$ is taking place. Usually orthoferrites are antiferromagnetic exhibiting very small spontaneous magnetization because of weak ferromagnetism (Eibschutz et al. 1967; Tsymbal et al. 2007).

The magnetic moments of rare-earth ions are aligned by exchange coupling with the transition metal (TM) subsystem (f–d exchange interaction), which results in a significant contribution to the low-temperature magnetic properties, as shown in Fig. 4b. The f–d exchange in a weak ferromagnetic phase of perovskite-type compounds is usually negative, i.e., the rare-earth magnetic moments are aligned antiparallel with respect to a ferromagnetic component associated with the TM magnetic sublattice, yielding negative magnetization at lowest temperatures, when the magnetic contribution of the rare-earth ions exceeds the ferromagnetic component of the TM sublattice (Khomchenko et al. 2008, 2009). However, in the case of $Bi_{1-x}Er_xFeO_3$ samples, a sharp increase in the magnetization observed with decreasing temperature suggests a positive f–d coupling.

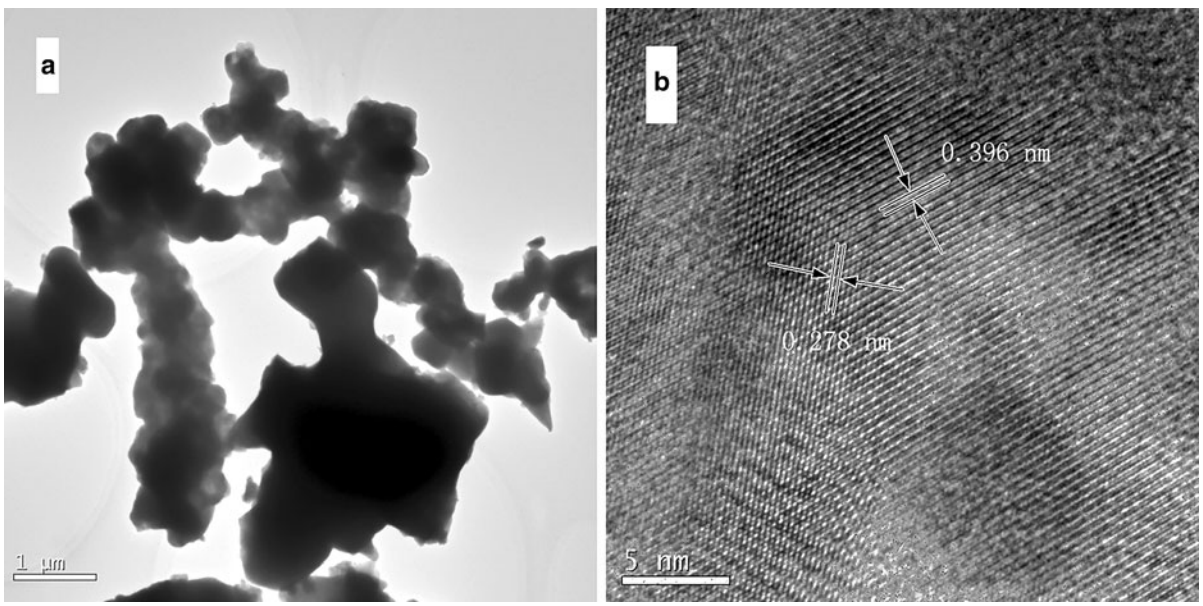

Fig. 3 TEM (**a**) and HRTEM (**b**) images of $Bi_{90}Er_{10}FeO_3$ nanoparticles left without stored in air

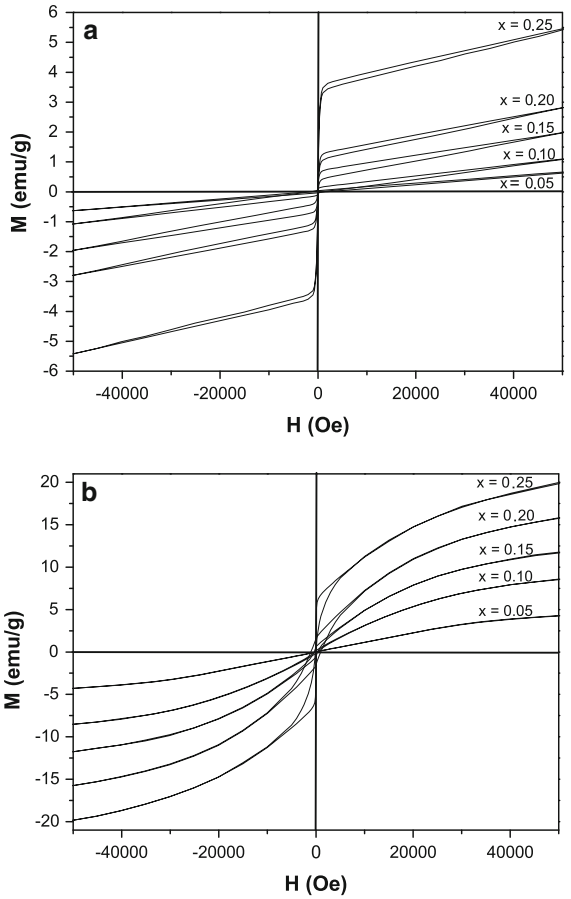

Fig. 4 *M–H* curves for $Bi_{1-x}Er_xFeO_3$ ($x = 0.05$, 0.10, 0.15, 0.20, 0.25) nanoparticles **a** at room temperature; **b** at 5 K

The enhanced ferromagnetic properties should be attributed to the substitution-induced suppression of the spiral spin modulation, which results from the fact that the radius of Er^{3+} is smaller than that of Bi^{3+}, leading to a larger distortion of lattice. Especially when the structure is changed from rhombohedral to orthorhombic symmetry, as revealed with the above XRD analysis, the spin cycloid of Er^{3+} will be destroyed, and therefore the latent magnetization locked within the cycloid might be released, resulting in the enhanced macroscopic magnetization as observed. Further, the enhanced ferromagnetism of Er^{3+}-doped $BiFeO_3$ nanoparticles may be similar to that of Eu^{3+}-doped nanoparticles. Using the first-principle calculations, we found that the magnetically active Er^{3+} ions coupled with Fe^{3+} ions can produce enhanced magnetism. Our ab initio calculations are performed using the accurate full potential projector augmented wave method, as implemented in the Vienna ab initio simulation package (VASP). They are based on the density functional theory with the generalized gradient approximation (GGA). The on-site Coulomb interaction is included in the GGA $+U$ approach with $U = 6.0$ eV and $J = 1.0$ eV for Fe 3d electrons. The fully relaxed crystal structure, which shows a R3c rhombohedral symmetry. In the mean time, antiferromagnetic configuration is the ground state, with 0.1569 eV/f.u. lower than the ferromagnetic one. For the effect of Er doping, we build up a $2 \times 2 \times 2$ supercell, with 80 atoms therein. One of Bi atoms is replaced by Er, which corresponds to 6.25 % doping. The on-site Coulomb interaction is included in the GGA + U approach with $U = 6.0$ eV and $J = 1.0$ eV for Er 4f electrons. It is found that Er^{3+} relaxes close to three Fe^{3+} ions and a ferromagnetic coupling between Er^{3+} and three Fe^{3+} is observed, leading to a pure magnetic moment of the system which is 9.4 μB. Since the effective magnetic moment of Er (9.4 μB) is larger than that of Eu (6 μB) (Liu et al. 2009), we propose that Er-doped $BiFeO_3$ nanoparticles can cause a greater magnetic enhancement.

The magnetization behavior as a function of temperature for all $Bi_{1-x}Er_xFeO_3$ samples at 1,000 Oe is shown in Fig. 5. For $x = 0.25$ at 5 K, the magnitude of Er moments is larger than that of Fe cations, and a ferromagnetic-like situation as revealed by ZFC curves as shown in Fig. 5 can occur. However, the moments of Er ions decrease with the increasing temperature, which accounts for the monotonical drop in magnetization up to 50 K. From 50 to 100 K, the ferromagnetism of Fe

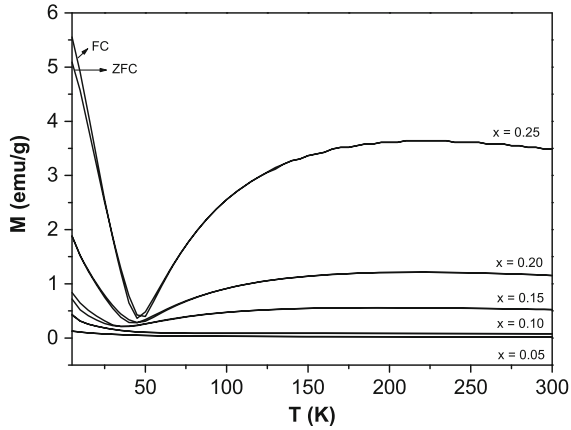

Fig. 5 ZFC/FC curves of $Bi_{1-x}Er_xFeO_3$ ($x = 0.05$, 0.10, 0.15, 0.20, 0.25) nanoparticles from 5 to 300 K with applied field 1,000 Oe

sublattice becomes prominent and ZFC curve tends to increases. Above 175 K, the magnetization becomes almost unchanged. Under a field larger than the local field that is suffered by the Er sublattice and produced by the Fe sublattice, the moments of Er will drive to be parallel to that of Fe, which results in the magnetization behavior as shown by the 1,000 Oe FC curve in Fig. 5. With the Er^{3+} concentration decrease from 10 %, the mentioned ferromagnetic interaction between the Er^{3+} and Fe^{3+} sublattices is neglected, and the Er sublattices can be considered as paramagnetic, i.e., the moments of Er^{3+} are aligned along the applied field. The macroscopic magnetization increases slowly as the temperature is decreasing to about 50 K, and then sharply rises up with further decreasing temperature.

Conclusion

A simple sol–gel method was used to synthesize $Bi_{1-x}Er_xFeO_3$ ($x = 0.05, 0.10, 0.15, 0.20, 0.25$) nanoparticles. The crystalline structure of $BiFeO_3$ changes from rhombohedral lattice to orthorhombic one by doping Er^{3+}. The improved ferromagnetic ordering of doped $BiFeO_3$ nanoparticles may be due to the substitution-induced suppression of the spiral spin modulation and the larger lattice distortion. The temperature dependence of magnetization for $Bi_{1-x}Er_xFeO_3$ is explained by the magnetic coupling between Er and Fe moments. The enhanced ferromagnetic moment of Er^{3+}-doped $BiFeO_3$ may make the materials applicable in fabricating multifunctional nanodevices at room temperature.

Acknowledgments This work was supported by the National Natural Science Foundation of China (Grant No. 11147101), the Natural Science Foundation of Henan (Grant Nos. 102102210448, 102102210452), and the Natural Science Foundation of Henan Department of Education (Grant No. 13A140806). The authors are grateful to Dr. Jiecai Fu of Lanzhou University for help with the TEM measurements. Dr. Zhao thanks Dr. Xingmin Cai and Dr. Fan Ye of School of Physical Science and Technology of Shenzhen University for helpful discussion.

References

Allibe J, Fusil S, Bouzehouane K, Daumont C, Sando D, Jacquet E, Deranlot C, Bibes M, Barthelemy A (2012) Room temperature electrical manipulation of giant magnetoresistance in spin valves exchange-biased with $BiFeO_3$. Nano Lett 12(3):1141–1145

Bhushan B, Das D, Priyam A, Vasanthacharya NY, Kumar S (2012) Enhancing the magnetic characteristics of $BiFeO_3$ nanoparticles by Ca, Ba co-doping. Mater Chem Phys 135(1):144–149

Du Y, Cheng Z, Yu Z, Dou SX, Wang X, Liu LQ (2012) Hydrothermal synthesized bismuth ferrites particles: thermodynamic, structural, and magnetic properties. J Nanosci Nanotechnol 12(2):1684–1687

Eibschutz M, Shtrikman S, Treves D (1967) Mössbauer studies of Fe^{57} in orthoferrites. Phys Rev 156(2):562–577

Giang DTH, Duc PA, Ngoc NT, Duc NH (2012) Geomagnetic sensors based on Metglas/PZT laminates. Sens Actuators A 179:78–82

Guo R, Fang L, Dong W, Zheng F, Shen M (2010) Enhanced photocatalytic activity and ferromagnetism in Gd doped $BiFeO_3$ nanoparticles. J Phys Chem C 114(49):21390–21396

Gupta HC, Singh MK, Tiwari LM (2002) Lattice dynamic investigation of Raman and infrared wavenumbers at the zone center of orthorhombic $RFeO_3$ (R = Tb, Dy, Ho, Er, Tm) perovskites. J Raman Spectrosc 33(1):67–70

Hur N, Jeong IK, Hundley MF, Kim SB, Cheong SW (2009) Giant magnetoelectric effect in multiferroic $HoMnO_3$ with a high ferroelectric transition temperature. Phys Rev B 79(13):134120

Khomchenko VA, Troyanchuk IO, Szymczak R, Szymczak H (2008) Negative magnetization in $La_{0.75}Nd_{0.25}CrO_3$ perovskite. J Mater Sci 43(16):5662–5665

Khomchenko VA, Shvartsman VV, Borisov P, Kleemann W, Kiselev DA, Bdikin IK, Vieira JM, Kholkin AL (2009) Effect of Gd substitution on the crystal structure and multiferroic properties of $BiFeO_3$. Acta Mater 57(17):5137–5145

Khomchenko VA, Paixao JA, Shvartsman VV, Borisov P, Kleemann W, Karpinsky DV, Kholkin AL (2010) Effect of Sm substitution on ferroelectric and magnetic properties of $BiFeO_3$. Scr Mater 62(5):238–241

Lebeugle D, Colson D, Forget A, Viret M, Bataille AM, Gukasov A (2008) Electric-field-induced spin flop in $BiFeO_3$ single crystals at room temperature. Phys Rev Lett 100(22):227602

Li YT, Zhang HG, Dong XG, Li Q, Mao WW, Dong CL, Ren SL, Li XA, Wei SQ (2013) Structural phase transition and magnetic properties of Er-doped $BiFeO_3$ nanoparticles. J Phys 430(1):012108

Liu J, Fang L, Zheng F, Ju S, Shen M (2009) Enhancement of magnetization in Eu doped $BiFeO_3$ nanoparticles. Appl Phys Lett 95(2):022511

Liu J, Li M, Pei L, Wang J, Yu B, Wang X, Zhao X (2010) Structural and multiferroic properties of the Ce-doped $BiFeO_3$ thin films. J Alloys Compd 493(1–2):544–548

Park TJ, Papaefthymiou GC, Viescas AJ, Moodenbaugh AR, Wong SS (2007) Size-dependent magnetic properties of single-crystalline multiferroic $BiFeO_3$ nanoparticles. Nano Lett 7(3):766–772

Prashanthi K, Chalke BA, Bapat RD, Purandare SC, Palkar VR (2010) Multiferroic $Bi_{0.7}Dy_{0.3}FeO_3$ thin films directly integrated on Si for integrated circuit compatible devices. Thin Solid Films 518(20):5866–5870

Ramesh R, Spaldin NA (2007) Multiferroics: progress and prospects in thin films. Nat Mater 6(1):21–29

Scott JF (2007) Data storage: multiferroic memories. Nat Mater 6(4):256–257

Selbach SM, Tybell T, Einarsrud MA, Grande T (2007) Size-dependent properties of multiferroic $BiFeO_3$ nanoparticles. Chem Mater 19(26):6478–6484

Seshadri R, Hill NA (2001) Visualizing the role of Bi 6s "lone pairs" in the off-center distortion in ferromagnetic $BiMnO_3$. Chem Mater 13(9):2892–2899

Singh MK, Jang HM, Gupta HC, Katiyar RS (2008) Polarized Raman scattering and lattice eigenmodes of antiferromagnetic $NdFeO_3$. J Raman Spectrosc 39(7):842–848

Szafraniak I, Polomska M, Hilczer B, Pietraszko A, Kepinski L (2007) Characterization of $BiFeO_3$ nanopowder obtained by mechanochemical synthesis. J Eur Ceram Soc 27(13–15):4399–4402

Tan GQ, Zheng YQ, Miao HY, Xia A, Ren HJ (2012) Controllable microwave hydrothermal synthesis of bismuth ferrites and photocatalytic characterization. J Am Ceram Soc 95(1):280–289

Tsymbal LT, Bazaliy YB, Derkachenko VN, Kameney VI, Kakazei GN, Palomares FJ, Wigen PE (2007) Magnetic and structural properties of spin-reorientation transitions in orthoferrites. J Appl Phys 101(12):123919

Wang J, Neaton JB, Zheng H, Nagarajan V, Ogale SB, Liu B, Viehland D, Vaithyanathan V, Schlom DG, Waghmare UV, Spaldin NA, Rabe KM, Wuttig M, Ramesh R (2003) Epitaxial $BiFeO_3$ multiferroic thin film heterostructures. Science 299(5613):1719–1722

Wu AH, Cheng GF, Shen H, Xu JY, Chu YQ, Ge ZW (2009) Preparation of $ReFeO_3$ nanocrystalline powders by auto-combustion of citric acid gel. Asia Pac J Chem Eng 4(5): 518–521

Wu J, Mao S, Ye ZG, Xie Z, Zheng L (2010) Room-temperature ferromagnetic/ferroelectric $BiFeO_3$ synthesized by a self-catalyzed fast reaction process. J Mater Chem 20(31): 6512–6516

Xie SH, Li JY, Proksch R, Liu YM, Zhou YC, Liu YY, Qu Y, Lan LN, Qiao Y (2008) Nanocrystalline multiferroic $BiFeO_3$ ultrafine fibers by sol-gel based electrospinning. Appl Phys Lett 93(22):222904

Yuan GL, Or SW, Liu JM, Liu ZG (2006) Structural transformation and ferroelectromagnetic behavior in single-phase $Bi_{1-x}Nd_xFeO_3$ multiferroic ceramics. Appl Phys Lett 89(5): 052905

Yuan GL, Qr SW, Chan HLW (2007) Raman scattering spectra and ferroelectric properties of $Bi_{1-x}Nd_xFeO_3$ ($x = 0$–0.2) multiferroic ceramics. J Appl Phys 101(6):064101

Zhang X, Sui Y, Wang X, Wang Y, Wang Z (2010) Effect of Eu substitution on the crystal structure and multiferroic properties of $BiFeO_3$. J Alloys Compd 507(1):157–161